NASA TN D-1606

TECHNICAL NOTE

D-1606

AERODYNAMIC CHARACTERISTICS AT A MACH NUMBER OF 6.77 OF A 9° CONE CONFIGURATION, WITH AND WITHOUT SPHERICAL AFTERBODIES, AT ANGLES OF ATTACK UP TO 180° WITH VARIOUS DEGREES OF NOSE BLUNTING

By Luther Neal, Jr.

Langley Research Center
Langley Station, Hampton, Va.

NATIONAL AERONAUTICS AND SPACE ADMINISTRATION
WASHINGTON
March 1963

NATIONAL AERONAUTICS AND SPACE ADMINISTRATION

TECHNICAL NOTE D-1606

AERODYNAMIC CHARACTERISTICS AT A MACH NUMBER OF 6.77 OF A 9° CONE CONFIGURATION, WITH AND WITHOUT SPHERICAL AFTERBODIES, AT ANGLES OF ATTACK UP TO 180° WITH VARIOUS DEGREES OF NOSE BLUNTING

By Luther Neal, Jr.

SUMMARY

Force and moment tests have been conducted on both sharp and spherical blunted cone configurations having semivertex angles of 9° in the Langley 11-inch hypersonic tunnel at a Mach number of 6.77, a Reynolds number per inch of 135,000, and an angle-of-attack range from 0° to 180°.

Analysis of the results indicates that a second stable trim condition can exist near $\alpha = 180^\circ$ for flat-base cone configurations depending upon the fineness ratio of the cone. However, it appears that this condition may be prevented by the addition to the basic cones of spherical afterbody caps whose centers of curvature coincide with the respective moment references.

A comparison of the experimental data with theory by using a combination of impact and modified Newtonian theory over different portions of the body shows that, except for the stable region at an angle of attack of 180° for the blunt cones, the method provides an adequate means of predicting the general trends of cone configurations throughout the entire 180° angle-of-attack range. Moreover, the actual magnitudes of the characteristics are predicted satisfactorily in many instances. At an angle of attack of 0°, however, the method significantly overpredicts the lift-curve slope C_{L_α} and the negative pitching-moment-curve slope C_{m_α} for the cones with large nose bluntness.

INTRODUCTION

In order to provide range control and to alleviate aerodynamic loading and heating during the reentry of a vehicle, the flight attitude can be modulated with time through large angles of attack. Also, unforeseen disturbances may be encountered which might cause the vehicle to tumble or reenter at random angles of attack. Therefore, in order to study this motion, it is important to know the aerodynamic characteristics of the vehicle for all possible flight attitudes. Furthermore, it is desirable to be able to predict these characteristics with

reasonable accuracy without conducting extensive wind-tunnel tests. Many different shapes, including various combinations of cones, cone frustums, and spherical noses or afterbodies, are used in the design of these reentry vehicles. The present investigation, however, is limited to a 9° semiangle cone configuration, with and without spherical afterbody caps, spherically blunted with nose bluntness ratios of 0, 0.32, and 0.65.

Considerable data are available on sharp as well as blunted cone configurations below an angle of attack of 60° (for example, see refs. 1 to 5); however, only a limited amount of information is available on cones at higher angles of attack. In reference 6, a comparison is made between theory and experiment for the aerodynamic characteristics up to an angle of attack of 130° at a Mach number of 6.8 for sharp cones with various semivertex angles, but no pitching-moment data are presented. A pressure study was reported on both sharp and blunted 5° and 15° semiangle cones at a Mach number of 3.9 in reference 7 up to an angle of attack of 100°. In the study reported in reference 8, pressure studies were conducted on a sharp and blunt 15° semiangle cone up to an angle of attack of 90° at $M = 6$. Force and moment characteristics for various cone configurations to an angle of attack of 180° are given in reference 9 for Mach numbers from 0.6 to 5.5 and in reference 10 for Mach numbers from 1.60 to 4.50.

Because of the scarcity of experimental force and moment data on cone configurations over a wide angle-of-attack range, the present investigation was undertaken. The purpose of this report is to present the results of this investigation and assess the ability of Newtonian theory to predict the experimental aerodynamic characteristics over an angle-of-attack range from 0° to 180°.

SYMBOLS

C_A axial-force coefficient, $\frac{\text{Axial force}}{q_\infty S}$

C_D drag coefficient, $\frac{\text{Drag}}{q_\infty S}$

C_L lift coefficient, $\frac{\text{Lift}}{q_\infty S}$

C_{L_α} lift-curve slope at $\alpha = 0°$, $\frac{dC_L}{d\alpha}$, per degree

$(C_L)_{max}$ maximum lift coefficient, $\frac{\text{Maximum lift}}{q_\infty S}$

C_m pitching-moment coefficient, $\frac{\text{Pitching moment}}{q_\infty SD}$

C_{m_α} pitching-moment-curve slope at $\alpha = 0^\circ$, $\frac{dC_m}{d\alpha}$, per degree

C_N normal-force coefficient, $\frac{\text{Normal force}}{q_\infty S}$

C_p pressure coefficient, $\frac{p - p_\infty}{q_\infty}$

$C_{p,max}$ maximum pressure coefficient behind normal shock

L/D lift-drag ratio

$(L/D)_{max}$ maximum lift-drag ratio

h/R nose bluntness ratio, ratio of vertical height between spherical nose tangency point and model center line to radius of base

D cone base diameter, in.

M_∞ free-stream Mach number

p pressure, lb/sq in.

p_∞ free-stream pressure, lb/sq in.

S cone base area, $\frac{\pi}{4} D^2$, sq in.

q_∞ free-stream dynamic pressure, lb/sq in.

α angle of attack (angle between model center line and wind vector), deg

γ ratio of specific heats

δ local flow deflection angle, deg

MODELS

Photographs of the various models used in the present investigation are shown in figure 1. Detail drawings of these models are presented in figure 2. Basically, the models consisted of 9° semivertex cones, with and without spherical afterbody caps, spherically blunted with nose bluntness ratios h/R of 0, 0.32, and 0.65. The centers of curvature for the spherical afterbody caps were selected so as to coincide with the moment reference location. All models were constructed of aluminum.

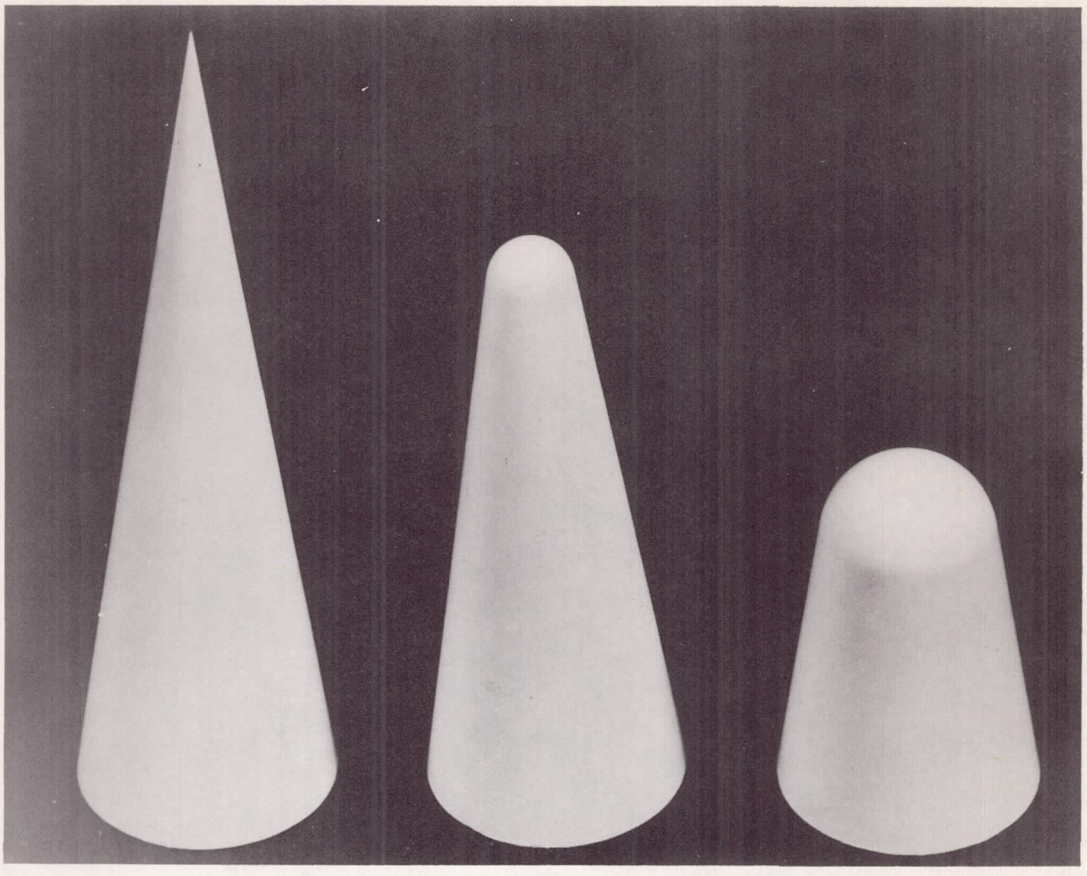

L-62-5008

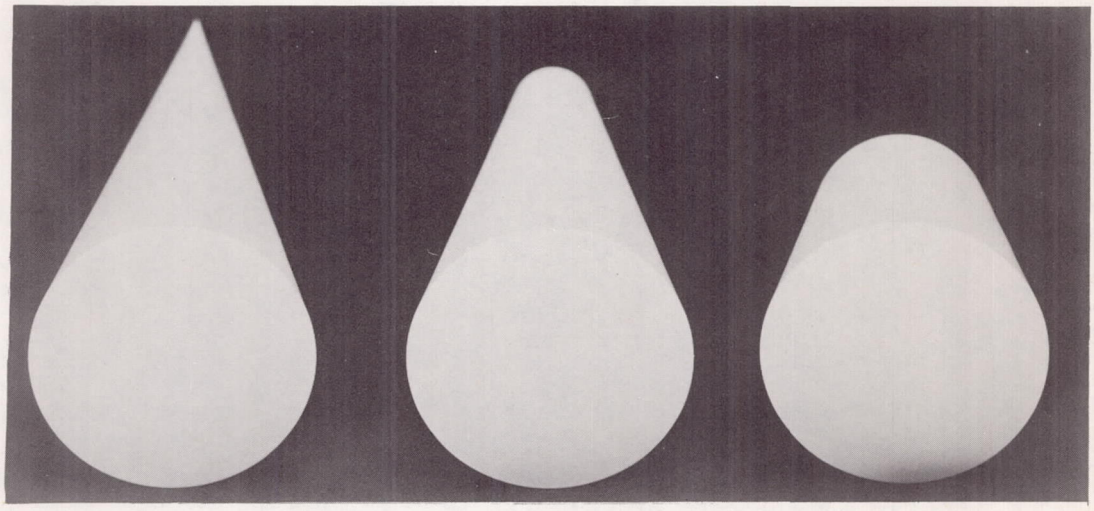

Figure 1.- Photographs of models. L-62-5009

Cones

Afterbodies

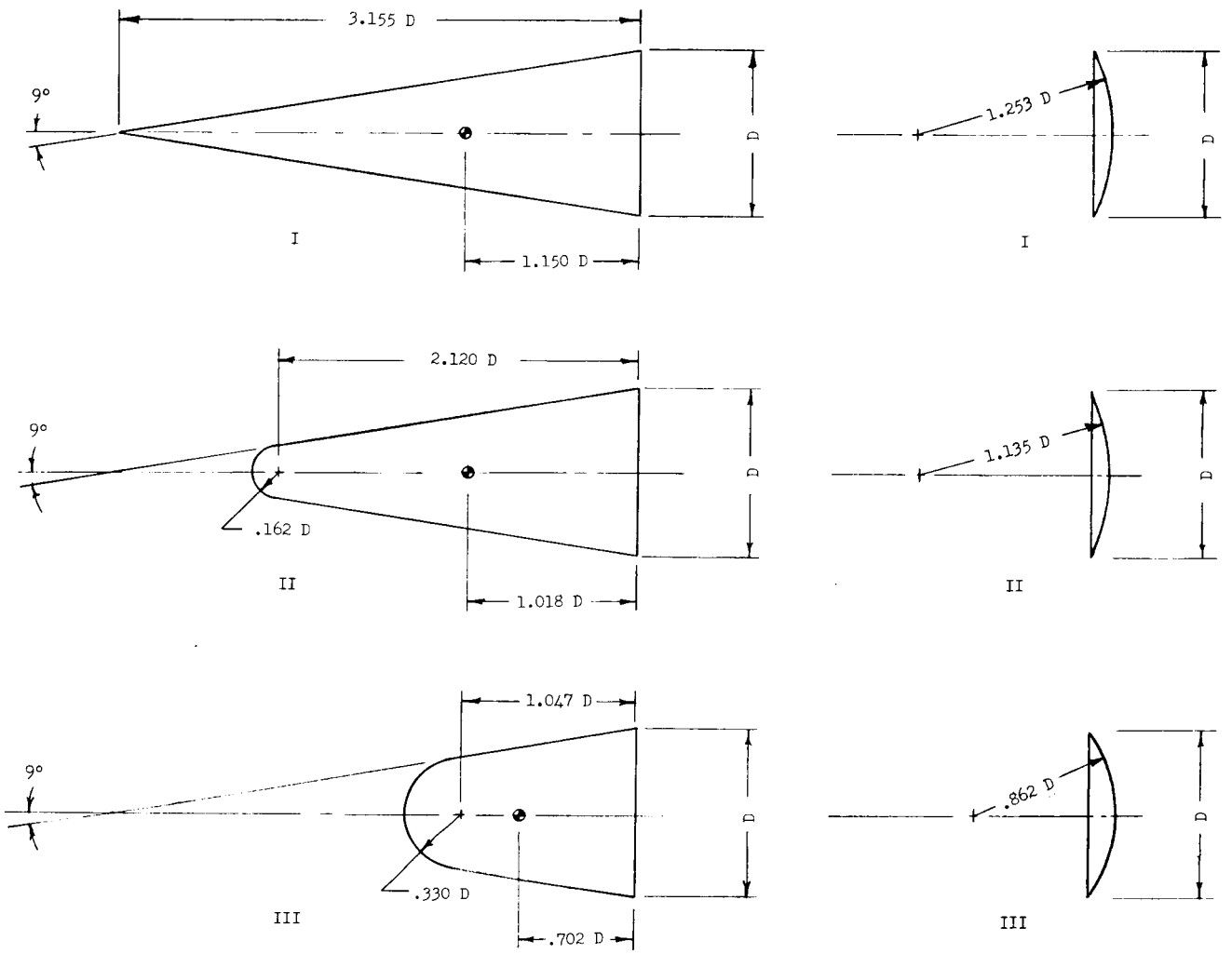

Cone model	Angle-of-attack range, deg	Dimension, D, in.
I	0 to 57	1.950
I	45 to 135	1.575
I	130 to 180	1.950
II and III	0 to 30	2.250
II and III	30 to 180	1.950

Figure 2.- Details of cones and afterbodies.

APPARATUS AND TESTS

Tunnel

The tests were conducted in the M = 6.8 Invar nozzle of the Langley 11-inch hypersonic tunnel. A description of the tunnel is given in reference 11 and a calibration of the nozzle in reference 12. Briefly, the tunnel is of the blowdown type and has a test duration from 60 to 90 seconds, depending on the stagnation pressure and model configuration. The test-section Mach number varies slightly with tunnel stagnation pressure because of changes in tunnel-wall boundary-layer thickness.

Tests

The present tests were conducted at a Mach number of 6.77, an average stagnation pressure of 10 atmospheres, and an average stagnation temperature of 550° F. This level of stagnation temperature was maintained in order to prevent the liquefaction of air in the test section. (See ref. 13.) The resulting Reynolds number corresponding to these test conditions was about 135,000 per inch.

A six-component strain-gage balance was used to measure the forces and moments on the model throughout the angle-of-attack range of 0° to 180°. The balance was inserted in the model at various angles to the model center line in order to cover the intended angle-of-attack range. These various initial angles, which may be observed in the schlieren photographs, presented later, were selected to minimize possible sting interference effects. The desired angles of attack were set by optical means in which a prism mounted on the model reflected a point source of light on a calibrated scale. This procedure allowed the true angle of attack to be obtained irrespective of any load deflection.

The moment reference for all cones was arbitrarily chosen to be 0.098 base diameters ahead of the centroid of planform area of the basic cones without spherical afterbodies.

The Mach number variation in the test-section region was ±0.03 or less. The free-stream Reynolds numbers did not vary more than ±10,000 per inch from the value previously given. The angles of attack are estimated to be accurate to ±0.2°. The variations in dynamic pressure due to slight changes in Mach numbers with time are about ±2 percent and were accounted for in the reduction of the data. No corrections are included in the data for the pressure acting inside the balance shield.

THEORETICAL METHODS

The longitudinal aerodynamic characteristics for the cone configurations were calculated throughout the angle-of-attack range of 0° to 180° by use of a combination of impact and modified Newtonian theory. The impact theory, based

on pure momentum consideration, assumes that the local pressure coefficient is given by the expression $C_p = 2 \sin^2\delta$, where δ is the local flow deflection angle. However, a modification to this theory is that in which the constant 2 is replaced by the maximum pressure coefficient behind a normal shock in order to improve the general agreement between theory and experiment in stagnation regions (ref. 14). This maximum pressure coefficient is given to good accuracy by Lee's approximate equation (ref. 15).

$$C_{p,max} = \frac{\gamma + 3}{\gamma + 1}\left[1 - \frac{2}{(\gamma + 3)M_\infty^2}\right]$$

For the present calculations, impact theory was used for the cone and cone frustums whereas a modified Newtonian theory was used for the spherical segments and flat base. In reference 6, it was noted that better agreement can be obtained by using a Newtonian coefficient of 2 for slender cones and $C_{p,max}$ for cones with larger included cone angles. Therefore, for the cone and cone frustums, a Newtonian coefficient of 2 seems reasonable since the present investigation involves a 9° semivertex cone. The use of $C_{p,max}$ in the calculations for the spherical segments seems justifiable from the standpoint of agreement with the stagnation values on the spherical segments. It was shown in reference 16 that modified Newtonian theory gives good prediction of the pressure distribution on a spherical segment. The overall integrated coefficients were computed by using the equations and tables given in reference 17 for bodies of this type.

RESULTS AND DISCUSSION

Basic Cone Data

The londitudinal force and moment characteristics referred to both the body- and stability-axis systems are shown in figures 3 and 4 for the various basic cones. Increasing the nose bluntness decreases both the normal force and negative pitching-moment coefficients (fig. 3) throughout the entire angle-of-attack range. Also, the axial-force coefficients increase with the nose bluntness below about 40°, decrease in the vicinity of 90°, and remain relatively unchanged above an angle of attack of 120°. At the extreme angles of attack (above 120°), the base contributes practically all the axial force and thus, since the reference area was the same for all cones, the axial-force coefficients are essentially not affected in this angle-of-attack region by blunting the nose.

Noteworthy in the variation of pitching-moment coefficients with angle of attack is the anomalous behavior near an angle of attack of 60° for all cones shown in figure 3. Similar anomalous results have been observed at lower angles of attack for cones and other bodies in the data for $M_\infty = 1.99$ reported in reference 18 and also in the data of reference 19 at about the same angle of attack for a 70° swept delta wing at $M_\infty = 6.8$. In addition, the data in references 9 and 10 show somewhat similar results at various supersonic Mach numbers for various cone configurations. As in reference 19, this anomalous behavior may be due to the flow between the shock and body changing from supersonic to subsonic in

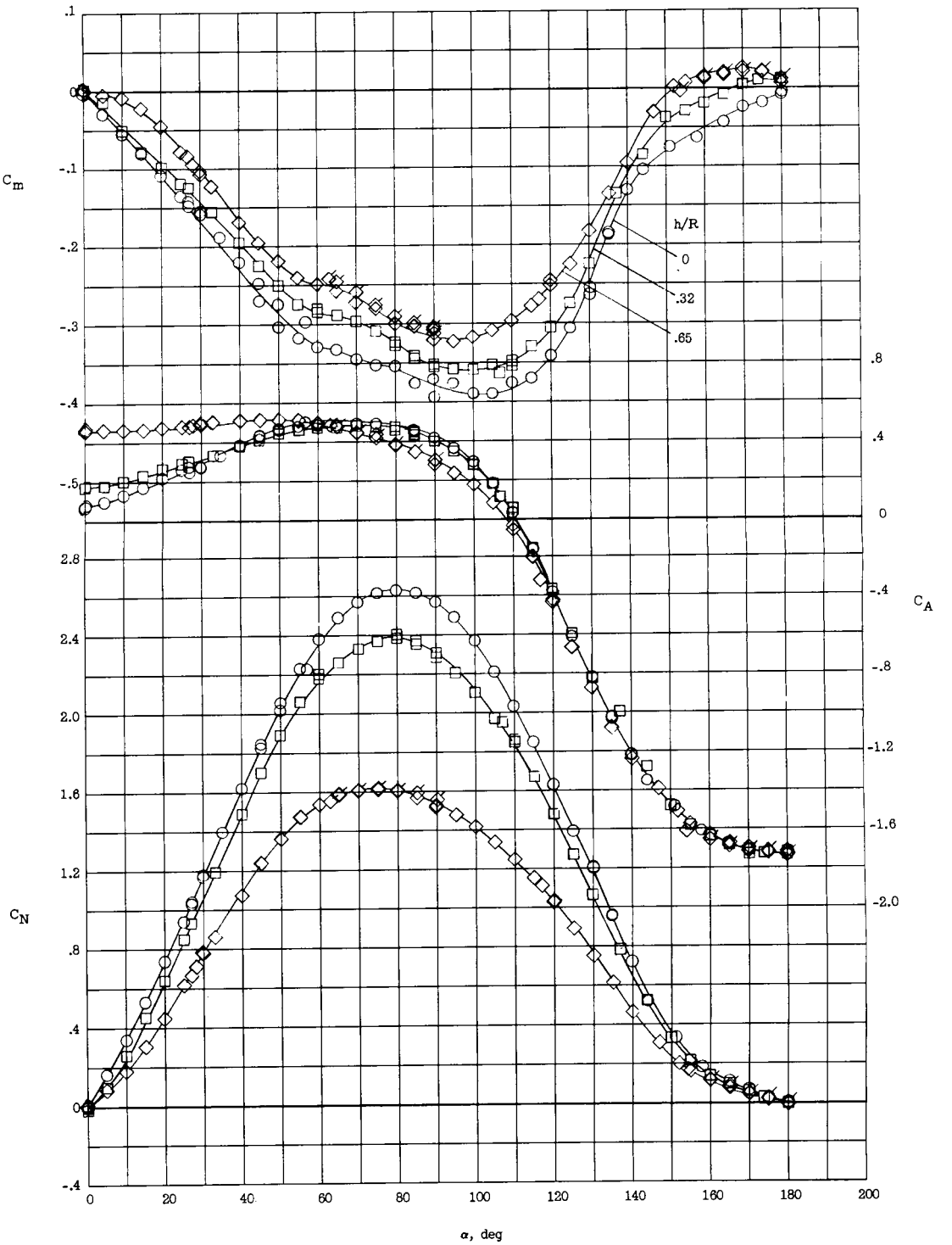

Figure 3.- Effects of nose bluntness on the longitudinal force characteristics referred to the body-axis system. Flagged symbols denote check runs.

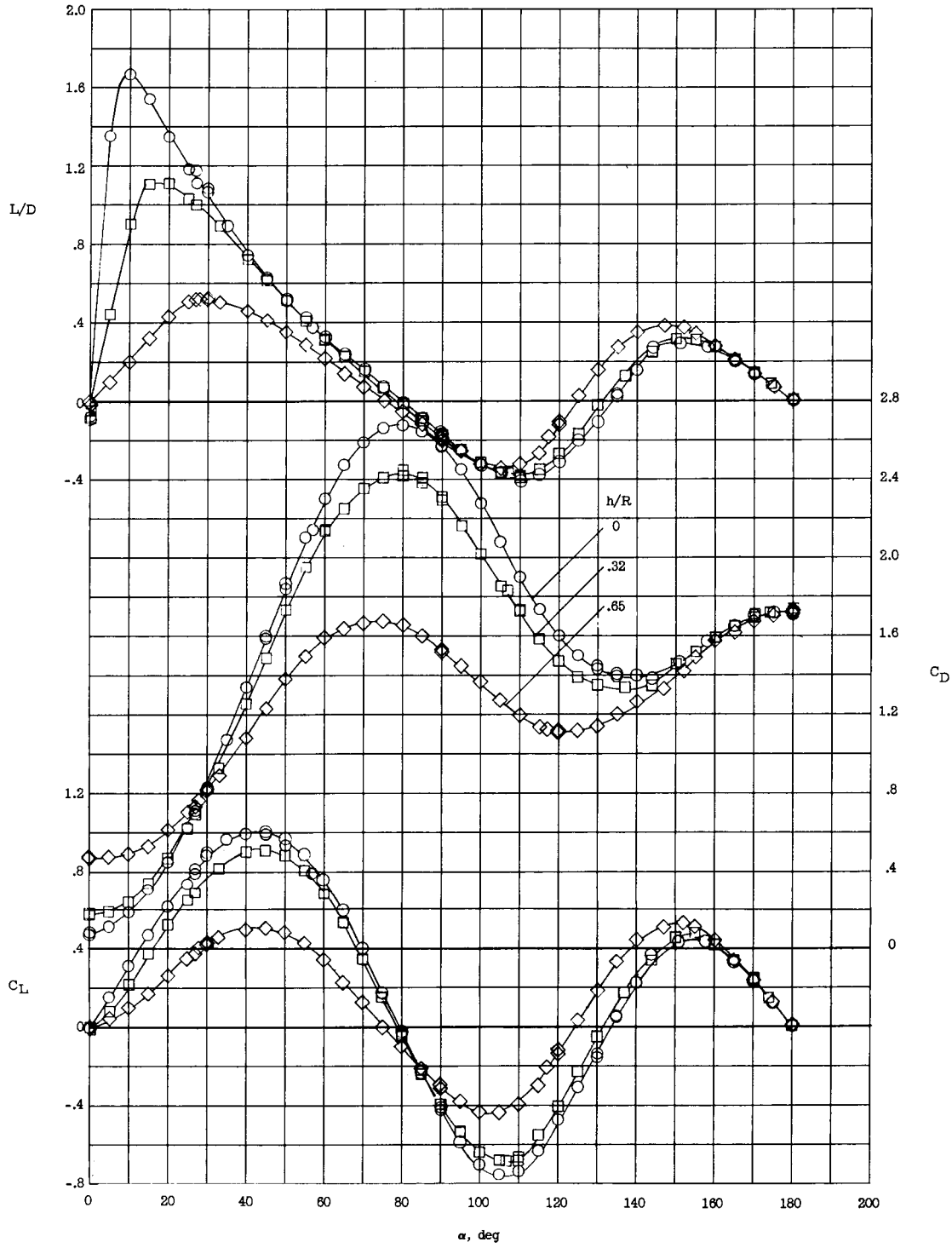

Figure 4.- Effects of nose bluntness on the longitudinal force characteristics referred to the stability-axis system.

this angle-of-attack range. The discrepancies in the pitching-moment coefficients for the sharp cone ($h/R = 0$) near an angle of attack of 50° for the two different sizes of models are not known.

In the extreme angle-of-attack range, a second stable trim condition near 180° exists for the blunter cones. This condition is mainly attributed to unsymmetrical pressure distribution over the flat base which is essentially the same for all cone fineness ratios; however, the sharp cone is unstable in this region. This is believed to occur because the pressures on the windward cone surface near the base provides a moment which becomes more effective for the sharper cones because of the longer pitch-moment arm involved and counteracts the stable inputs from the cone base.

The effects of nose bluntness on the lift and drag characteristics are shown in figure 4. For all bluntness ratios, maximum positive ($\alpha < 90^\circ$) and negative lift is obtained at angles of attack of about 45° and 105°, respectively. For the bluntness ratios considered here, increasing the bluntness results in drag increases up to an angle of attack of about 25°. Maximum values of L/D are decreased considerably by blunting the cone whereas above an angle of attack of 60°, L/D values are affected to a lesser degree.

Comparison of Basic Data With Theory

The longitudinal force and moment characteristics, referred to both the body- and stability-axis systems, are compared with theory in figures 5 and 6. In general, the theory gives good predictions of the overall trends throughout the entire angle-of-attack range. There are, however, regions of appreciable deviations between theory and experiment which should be noted. For example, the anomalous behavior in pitching moment at an angle of attack near 60° (fig. 5) is unpredicted. As mentioned previously, this behavior may be due to the onset of subsonic flow between the shock and body in this angle-of-attack range. When this occurs, cone surface pressure "bleed-off" near the base can become appreciable and result in the experimental trends shown. The theory, of course, does not account for this pressure bleed-off and overpredicts the data. References 7 and 8 which contain local-pressure information at these angles of attack do not clearly show this pressure bleed-off near the base. This is not conclusive evidence that this effect is not present on cones, however, since pressure measurements were not made within the last 6 percent and 11 percent of the cone length in references 7 and 8, respectively. This anticipated reduction in pressure near the base of the cone may also have caused the deviation in experimental and predicted normal-force coefficients (see fig. 5) in this particular angle-of-attack range ($55^\circ < \alpha < 90^\circ$).

At the extreme angles of attack (near 180°), bleed-off in pressure around the edge of the cone base becomes appreciable and thus the axial force is overpredicted by theory. As mentioned before, in this extreme angle-of-attack range, unsymmetrical pressure distribution over the flat base appears to produce a second stable trim condition near 180° for the blunter cones. In reference 9, a second stable trim condition was also noted for similar low-fineness-ratio configurations. Thus, should a cone configuration with a flat base reverse itself or tumble because of some unforeseen disturbance, the vehicle might stabilize in a backward attitude during reentry. With this in mind, spherical afterbody caps

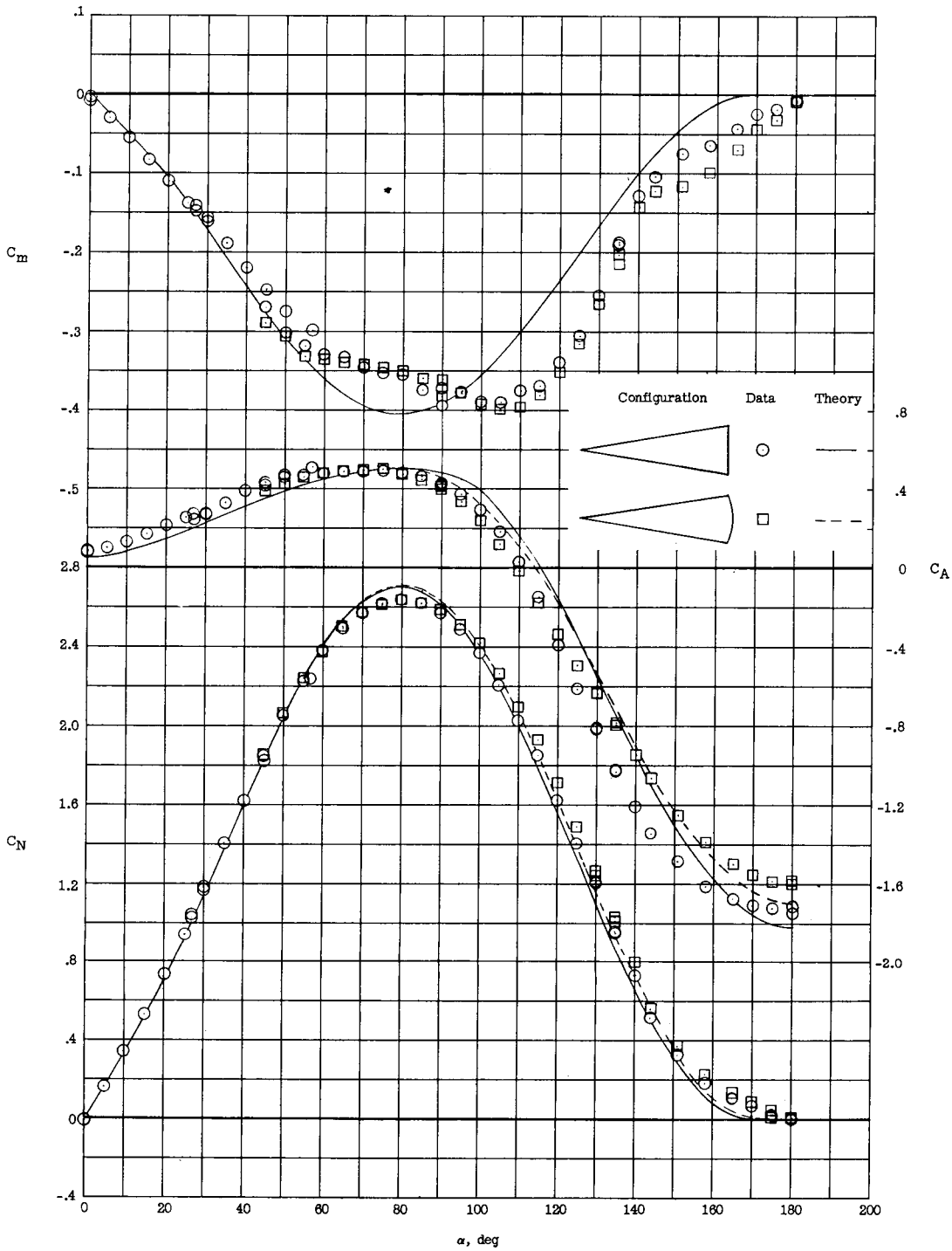

(a) Cone I; afterbody I; h/R = 0.

Figure 5.- Comparison with theory of the longitudinal force characteristics referred to the body-axis system for cones of various bluntnesses with and without afterbodies.

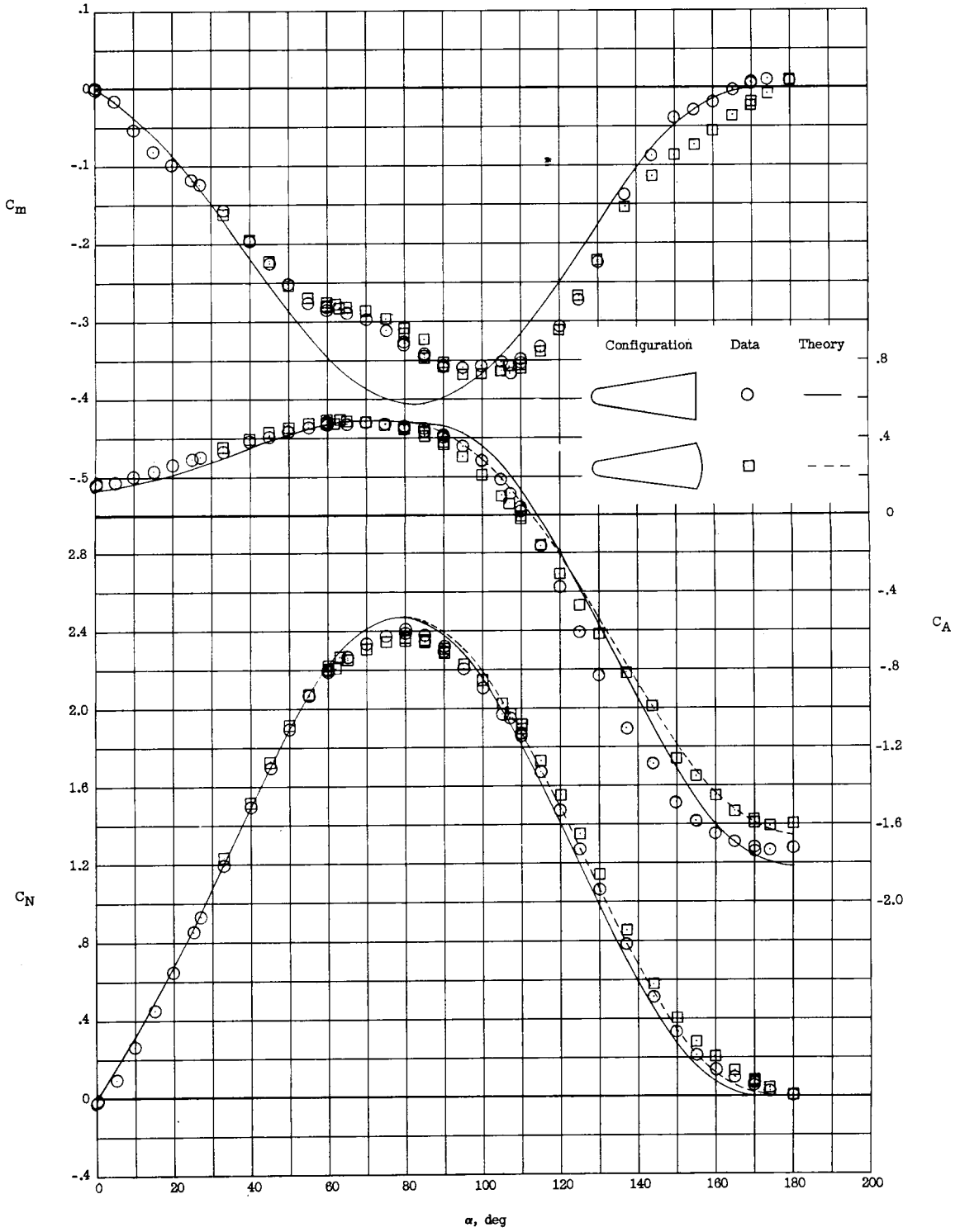

(b) Cone II; afterbody II; h/R = 0.32.

Figure 5.- Continued.

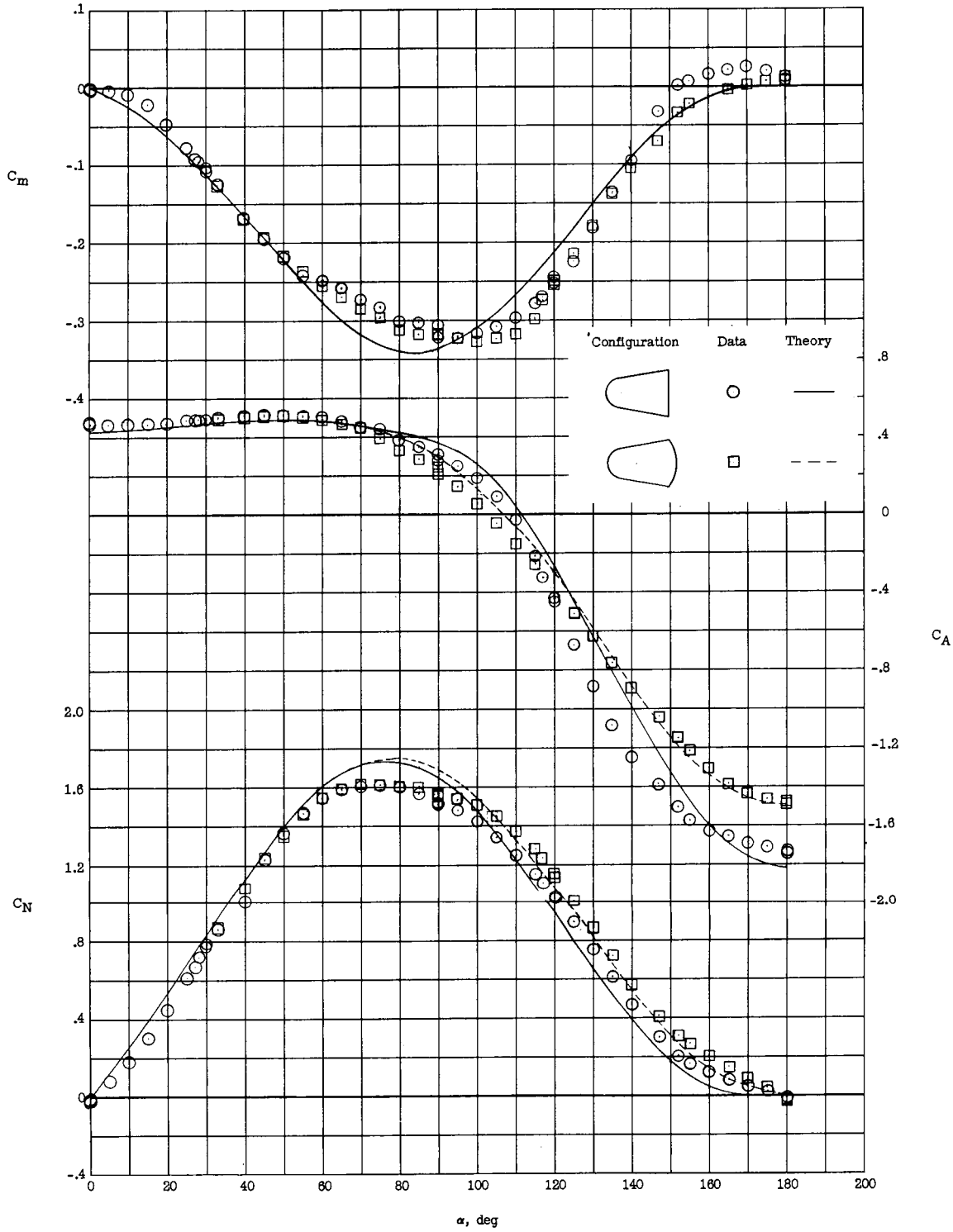

(c) Cone III; afterbody III; h/R = 0.65.

Figure 5.- Concluded.

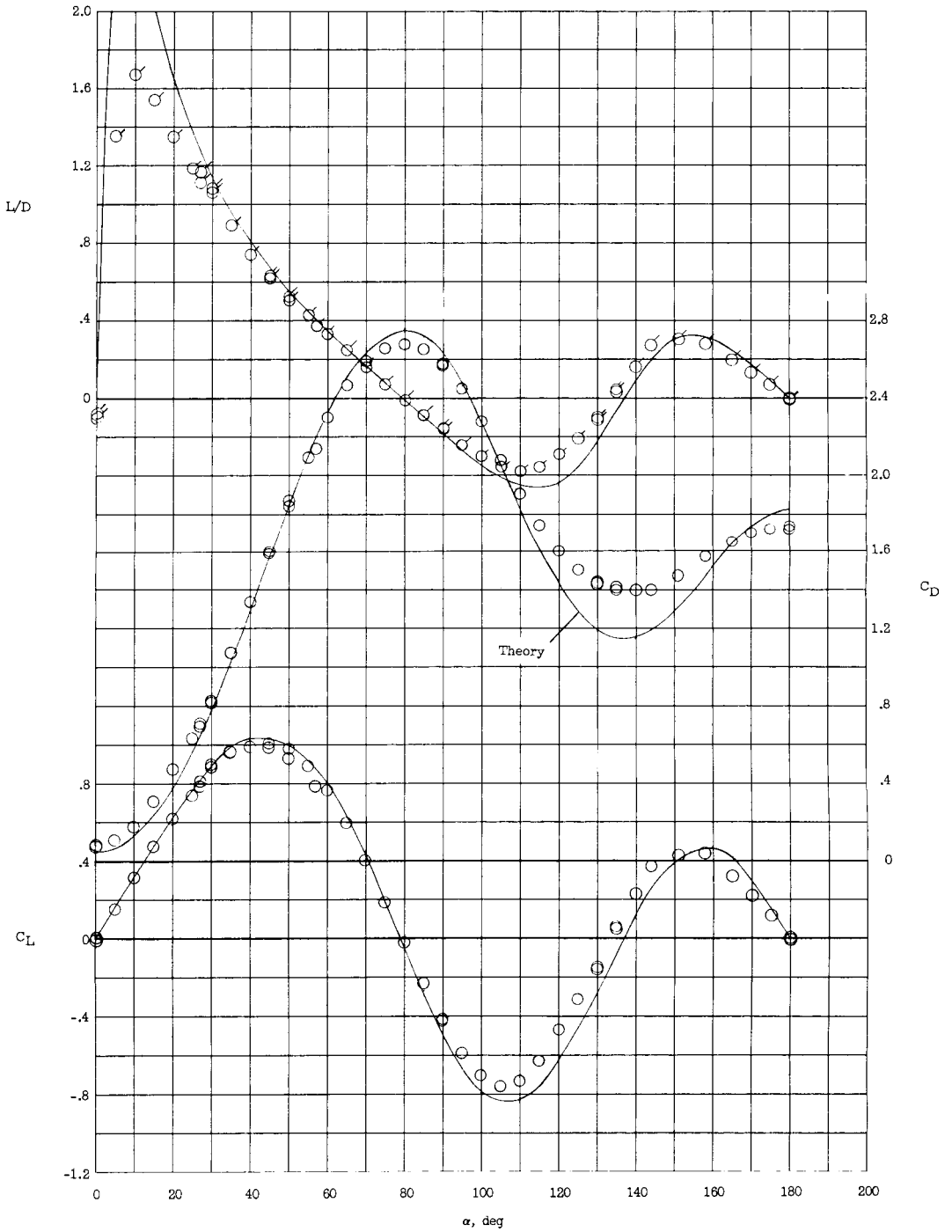

(a) Cone I; h/R = 0. L/D values are denoted by the flagged symbols in this part.

Figure 6.- Comparison with theory of the longitudinal force characteristics referred to the stability-axis system for cones with various nose bluntnesses.

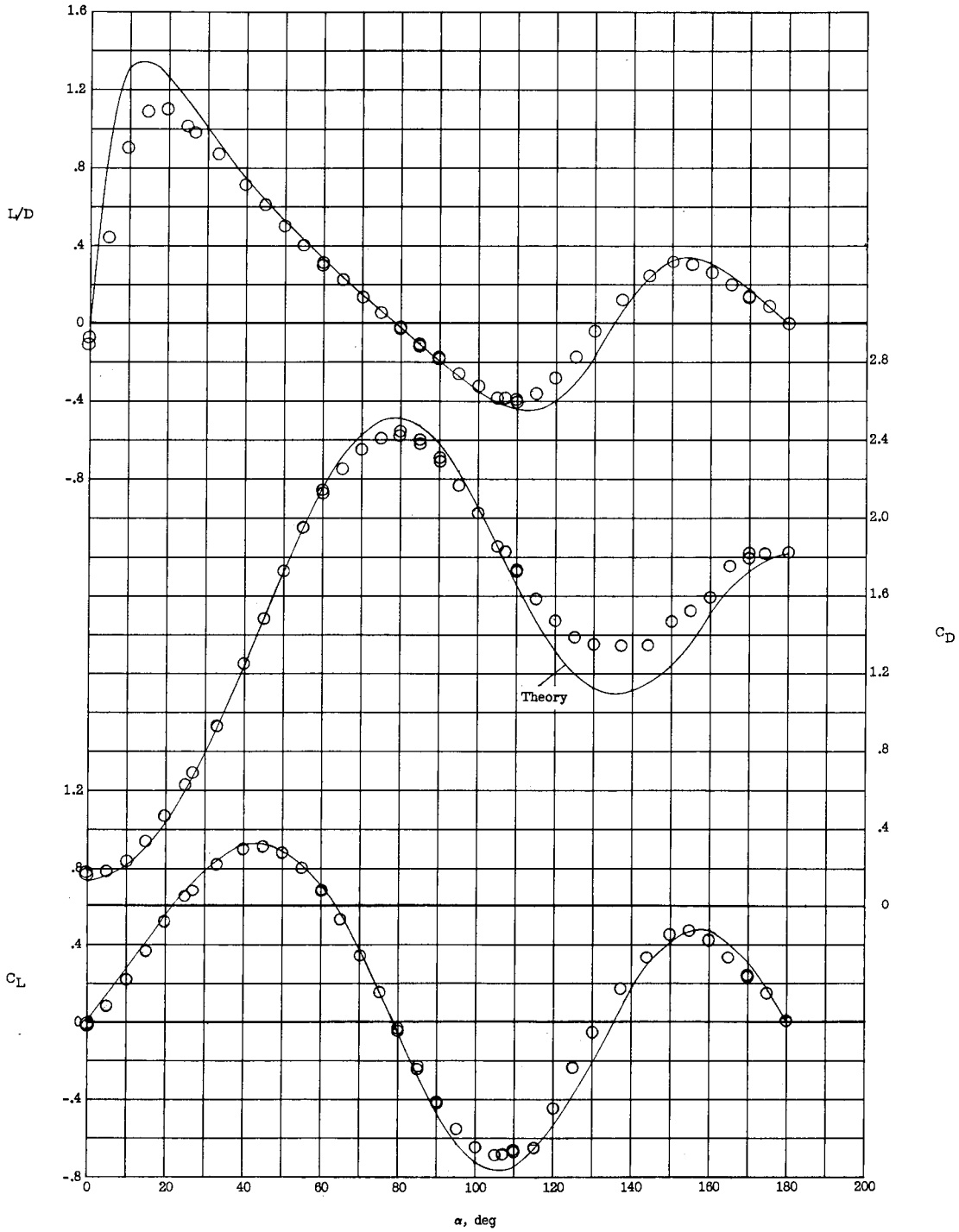

(b) Cone II; h/R = 0.32.

Figure 6.- Continued.

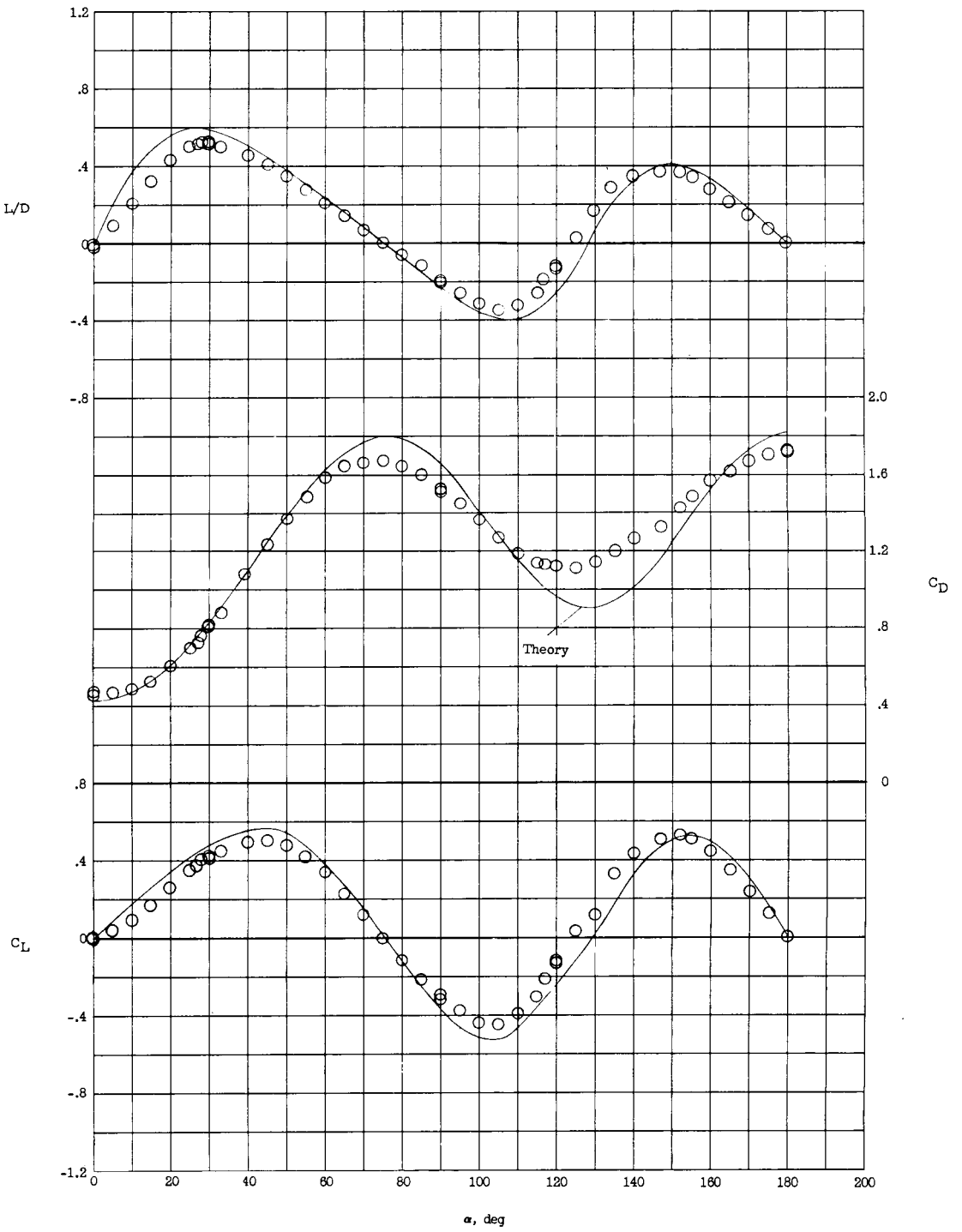

(c) Cone III; h/R = 0.65.

Figure 6.- Concluded.

were designed whose centers of curvature coincided with the moment reference of the basic cones. Thus, theoretically at least, no pitching moment is produced by the spherical cap since all forces on the cap act through the moment reference. The cap may, however, change the shape of the shock and indirectly affect the pressure distribution over other parts of the configuration. Experimental data for these cone-afterbody configurations are also shown in figure 5. The data indicate that such afterbodies provide an effective means of eliminating the likely second stable trim condition near $\alpha = 180^\circ$ on flat-base cone configurations. At angles of attack below 140°, only small changes in the pitching-moment coefficients are noted with the addition of the spherical afterbodies.

Generally, the increment in normal-force coefficient due to the afterbodies appears to be predicted fairly well throughout the angle-of-attack range (fig. 5). Also, the axial-force coefficients are, in general, better predicted for the cone-afterbody configurations than for the basic cones. No increment in the pitching-moment coefficient is predicted since all forces on the spherical cap are directed through the moment reference.

The lift and drag characteristics for the basic cones are compared with theory in figure 6. General examination of the figures reveals that theory gives excellent predictions of the trends throughout the entire angle-of-attack range. Moreover, closer examination shows that the maximum positive and negative values of C_L, C_D, and L/D with respect to angle of attack are predicted very well and, in many cases, the actual magnitudes of these characteristics are satisfactorily predicted. For the sharper cones, $(L/D)_{max}$ is overpredicted because viscous forces have been neglected by the theory; on these shapes the contribution of viscous forces can amount to a significant portion of the total drag and thereby lower $(L/D)_{max}$. The minimum peak in C_D at angles of attack between 120° and 140° is underpredicted by theory. This result stems from the fact that Newtonian theory characteristically underpredicts the forces on flat surfaces (the base) at small flow deflection angles.

Effects of Nose Bluntness on C_{m_α}, C_{L_α}, $(L/D)_{max}$, and $(C_L)_{max}$

The effects of nose bluntness on C_{m_α}, C_{L_α}, $(C_L)_{max}$, and $(L/D)_{max}$ are shown in figure 7. Both data and theory show a decrease in C_{L_α} and negative C_{m_α} with increases in nose bluntness. Both of these parameters are predicted very well for the sharp cone; however, the experimental data show a much greater drop off with increases in nose bluntness than is indicated by theory. For $h/R = 0.65$, C_{L_α} is overpredicted by about 100 percent and negative C_{m_α} is overpredicted by about 200 percent. For all bluntness ratios, $(C_L)_{max}$ $(\alpha < 90^\circ)$ is predicted very well by theory. However, maximum lift-drag ratio is overpredicted considerably for the sharper cones because the theory used neglected viscous forces. It was shown for cones in reference 6 that much closer agreement between theory and experiment for $(L/D)_{max}$ is obtained when skin friction is accounted for.

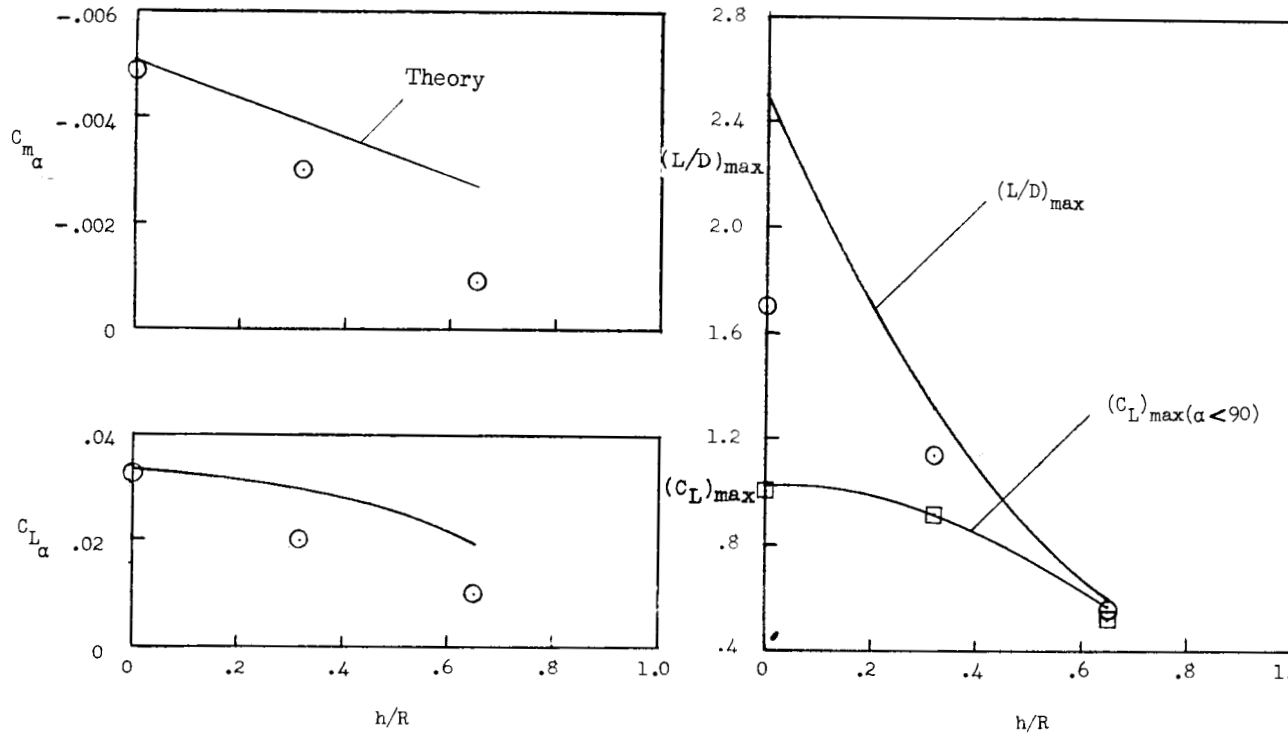

Figure 7.- Comparison between theory and experiment for C_{m_α}, C_{L_α}, $(L/D)_{max}$, and $(C_L)_{max}$ for various bluntness ratios.

Schlieren Photographs

Typical schlieren photographs are shown in figures 8 and 9 for the various configurations tested. As expected, considerable changes in the shock shapes are obtained at an angle of attack of 0° by blunting the cone. At the higher angles of attack, however, blunting the cone appears generally to affect the shape of the shock only near the nose region of the model. The bow shock is essentially straight for the sharp cone up to angles of attack of about 55° and for the blunt cones from angles of attack of approximately 20° to 55°. Above 55° shock curvature begins to occur; this condition indicates the onset of subsonic flow between the bow shock and the body which can result in appreciable pressure bleed-off near the cone base as discussed previously.

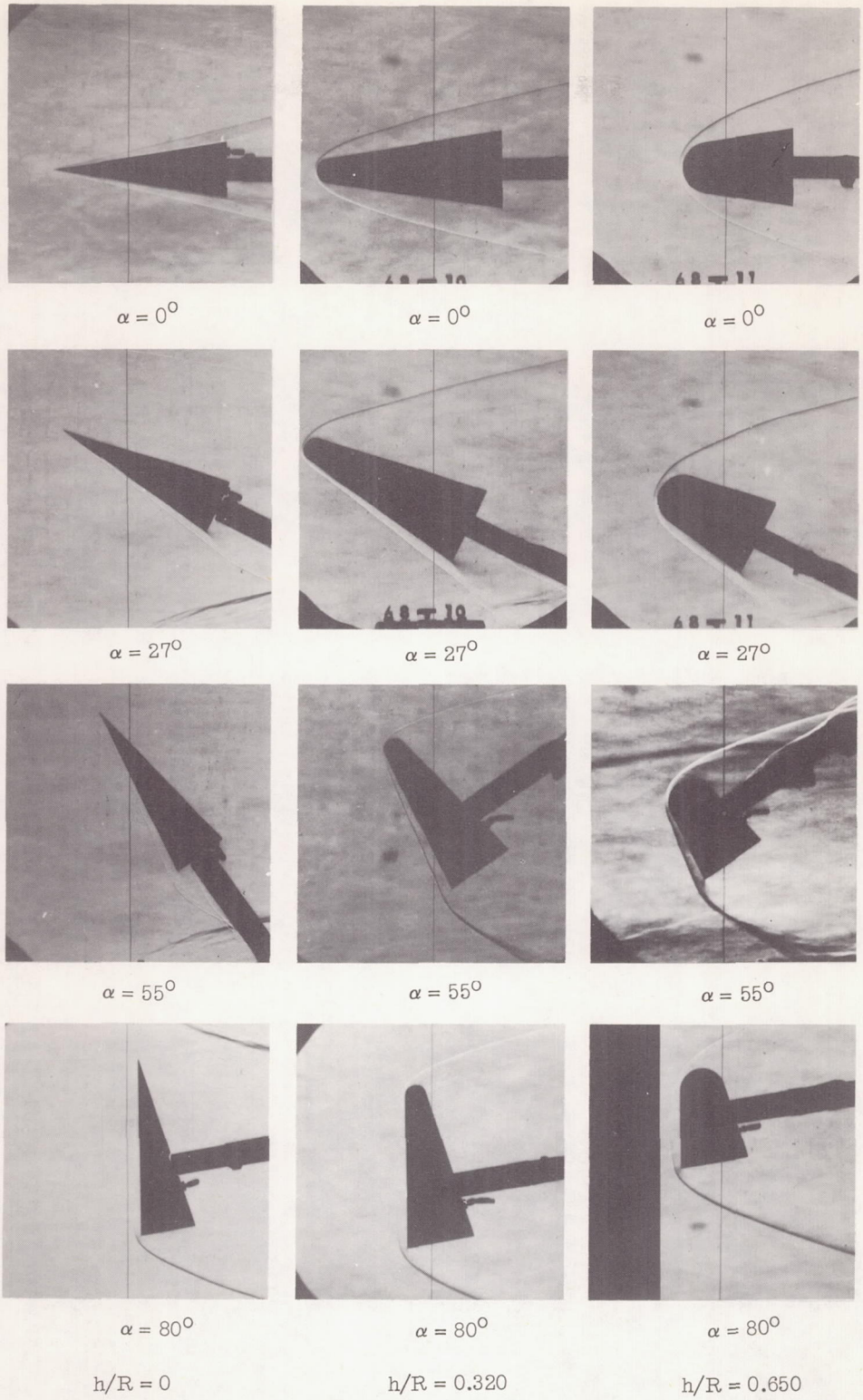

Figure 8.- Schlieren photographs of basic cone models. L-62-7050

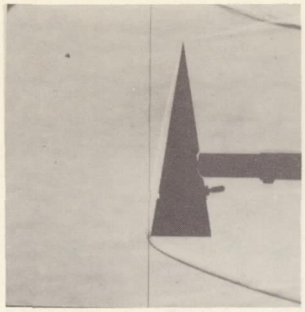

$\alpha = 90^{\circ}$

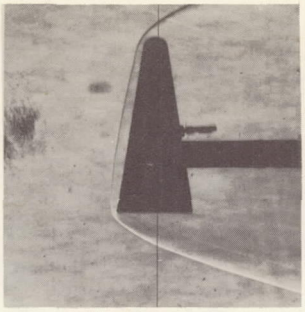

$\alpha = 90^{\circ}$

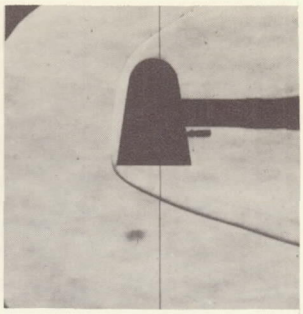

$\alpha = 90^{\circ}$

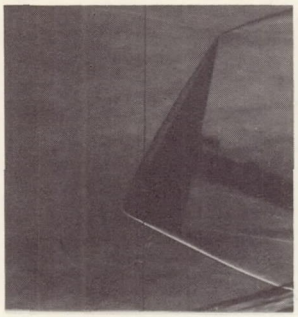

$\alpha = 110^{\circ}$

$\alpha = 105^{\circ}$

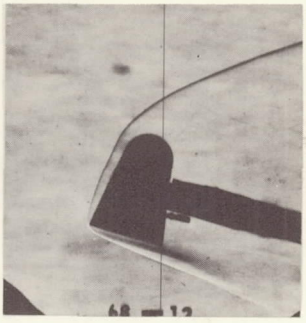

$\alpha = 105^{\circ}$

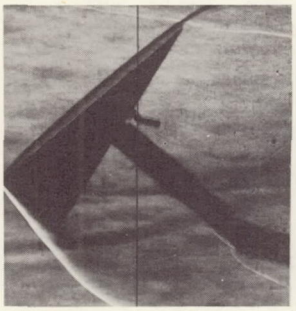

$\alpha = 130^{\circ}$

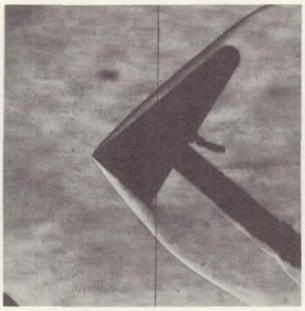

$\alpha = 130^{\circ}$

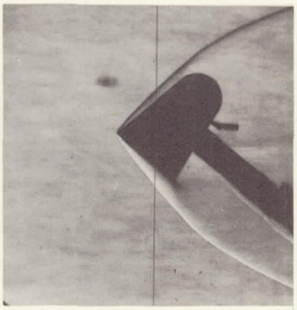

$\alpha = 130^{\circ}$

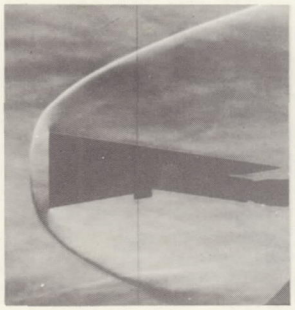

$\alpha = 180^{\circ}$

h/R = 0

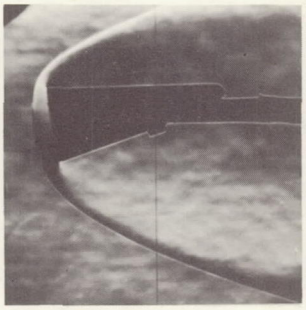

$\alpha = 170^{\circ}$

h/R = 0.320

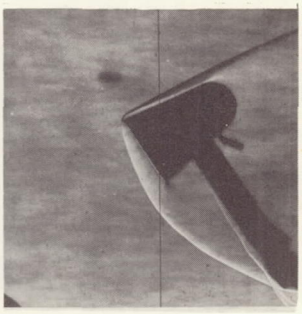

$\alpha = 147^{\circ}$

h/R = 0.650

Figure 8.- Concluded. L-62-7051

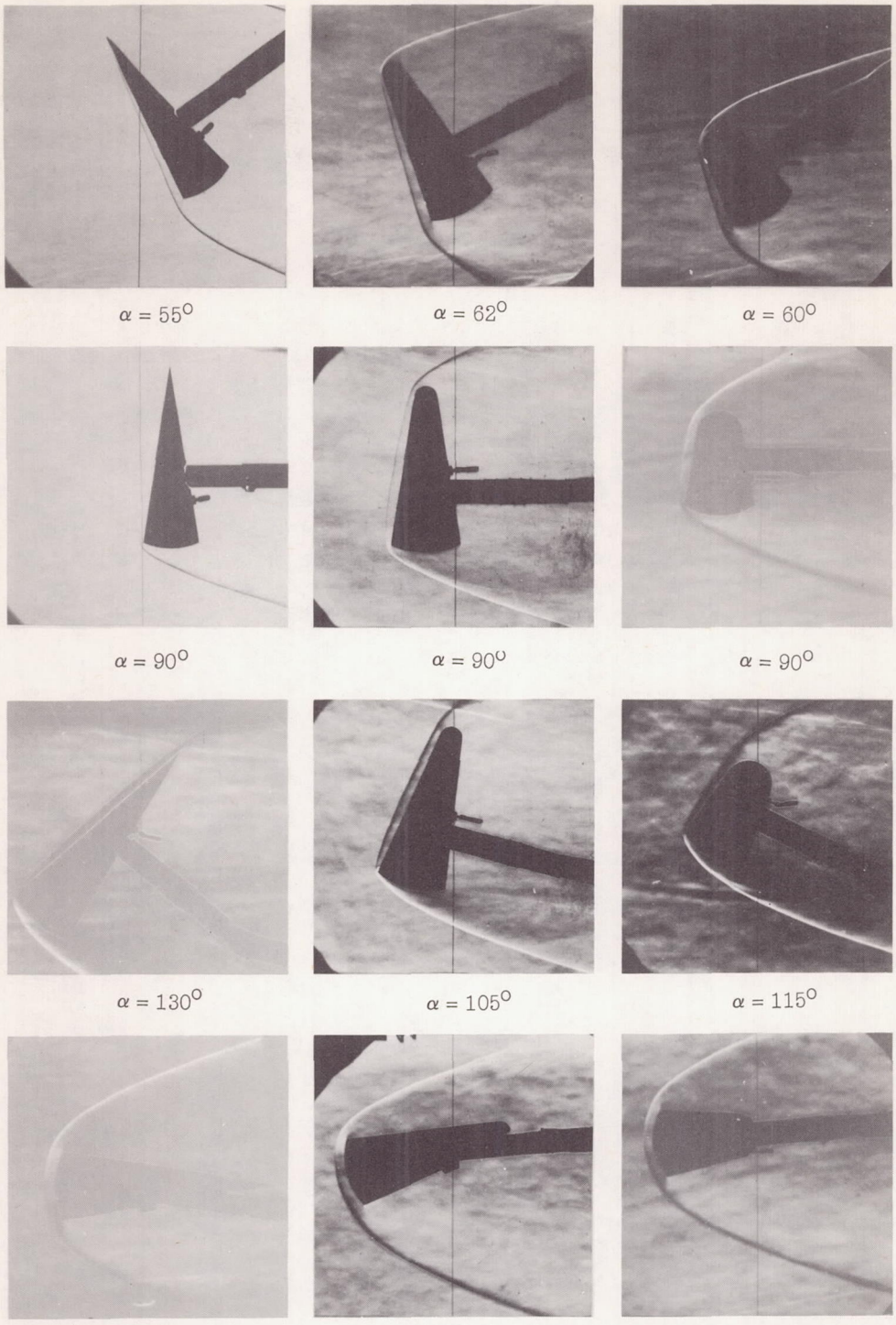

Figure 9.- Schlieren photographs of the models with afterbodies. L-62-7052

CONCLUSIONS

The following conclusions were obtained from the analysis of force and moment test results at a Mach number of 6.77, a Reynolds number per inch of 135,000, and an angle-of-attack range from 0° to 180° on both sharp and spherical blunted cone configurations having semivertex angles of 9°:

1. A second stable trim condition occurs near $\alpha = 180^\circ$ for flat-base cone configurations of low fineness ratio.

2. The addition of spherical afterbody caps whose centers of curvature coincide with the respective moment reference eliminates this second trim condition.

3. A comparison of the experimental data with theory using a combination of impact and modified Newtonian theory over different portions of the body shows that, except for the stable region at an angle of attack of 180° for the blunt cones, the method provides an adequate means of predicting the general trends of cone configurations throughout the entire 180° angle-of-attack range. Moreover, the magnitudes of the characteristics are predicted satisfactorily in many instances. At an angle of attack of 0°, however, the method significantly overpredicts the lift-curve slope C_{L_α} and negative pitching-moment-curve slope C_{m_α} for the cones with large nose bluntness.

Langley Research Center,
National Aeronautics and Space Administration,
Langley Station, Hampton, Va., November 14, 1962.

REFERENCES

1. Armstrong, William O.: Hypersonic Aerodynamic Characteristics of Several Series of Lifting Bodies Applicable to Reentry Vehicle Design. NASA TM X-536, 1961.

2. Dennis, David H., and Cunningham, Bernard E.: Forces and Moments on Pointed and Blunt-Nosed Bodies of Revolution at Mach Numbers From 2.75 to 5.00. NACA RM A52E22, 1952.

3. Fitch, C. R., Morris, S. D., and Dunkin, O. L.: Force, Pressure, and Heat Transfer Tests of the GE Skybolt Nose Cone at Mach 10. AEDC-TDR 62-125 (Contract No. AF40(600)-800 S/A 24(61-73)), Arnold Eng. Dev. Center, June 1962.

4. Savin, Raymond C.: Application of the Generalized Shock-Expansion Method to Inclined Bodies of Revolution Traveling at High Supersonic Airspeeds. NACA TN 3349, 1955.

5. Jorgensen, Leland H.: Elliptic Cones Alone and With Wings at Supersonic Speeds. NACA Rep. 1376, 1958. (Supersedes NACA TN 4045.)

6. Penland, Jim A.: Aerodynamic Force Characteristics of a Series of Lifting Cone and Cone-Cylinder Configurations at a Mach Number of 6.83 and Angles of Attack up to 130°. NASA TN D-840, 1961.

7. Amick, James L.: Pressure Measurements on Sharp and Blunt 5°- and 15°-Half-Angle Cones at Mach Number 3.86 and Angles of Attack to 100°. NASA TN D-753, 1961.

8. Conti, Raul J.: Laminar Heat-Transfer and Pressure Measurements at a Mach Number of 6 on Sharp and Blunt 15° Half-Angle Cones at Angles of Attack up to 90°. NASA TN D-962, 1961.

9. Treon, Stuart L.: Static Aerodynamic Characteristics of Short Blunt Cones With Various Nose and Base Cone Angles at Mach Numbers From 0.6 to 5.5 and Angles of Attack to 180°. NASA TN D-1327, 1962.

10. Turner, Kenneth L., and Shaw, David S.: Wind-Tunnel Investigation at Mach Numbers From 1.60 to 4.50 of the Static-Stability Characteristics of Two Nonlifting Vehicles Suitable for Reentry. NASA MEMO 3-2-59L, 1959.

11. McLellan, Charles H., Williams, Thomas W., and Bertram, Mitchel H.: Investigation of a Two-Step Nozzle in the Langley 11-Inch Hypersonic Tunnel. NACA TN 2171, 1950.

12. Bertram, Mitchel H.: Exploratory Investigation of Boundary-Layer Transition on a Hollow Cylinder at a Mach Number of 6.9. NACA Rep. 1313, 1957. (Supersedes NACA TN 3546.)

13. McLellan, Charles H., and Williams, Thomas W.: Liquefaction of Air in the Langley 11-Inch Hypersonic Tunnel. NACA TN 3302, 1954.

14. Penland, Jim A.: Aerodynamic Characteristics of a Circular Cylinder at Mach Number 6.86 and Angles of Attack up to 90°. NACA TN 3861, 1957. (Supersedes NACA RM L54A14.)

15. Lees, Lester: Hypersonic Flow. Fifth International Aeronautical Conference (Los Angeles, Calif., June 20-23, 1955), Inst. Aero, Sci., Inc., 1955, pp. 241-276.

16. Lees, Lester: Recent Developments in Hypersonic Flow. Jet Propulsion, vol. 27, no. 11, Nov. 1957, pp. 1162-1178.

17. Wells, William R., and Armstrong, William O.: Tables of Aerodynamic Coefficients Obtained From Developed Newtonian Expressions for Complete and Partial Conic and Spheric Bodies at Combined Angles of Attack and Sideslip With Some Comparisons With Hypersonic Experimental Data. NASA TR R-127, 1962.

18. Jackson, Charlie M., Jr., and Harris, Roy V., Jr.: Investigation at a Mach Number of 1.99 of Two Series of Blunted Delta Planform Models With Several Cross-Sectional Shapes for Angles of Attack From 0° to 90°. NASA TM X-543, 1961.

19. Fetterman, David E. and Neal, Luther, Jr.: An Analysis of the Delta-Wing Hypersonic Stability and Control Behavior at Angles of Attack Between 30° and 90°. NASA TN D-1602, 1963.

NASA-Langley, 1963 L-3173